

Mechanically induced metal–insulator transition in carbyne

Vasilii I. Artyukhov and Mingjie Liu

Department of Mechanical Engineering and Materials Science, Rice University, Houston, Texas 77005

Boris I. Yakobson

*Department of Mechanical Engineering and Materials Science,
Department of Chemistry and Smalley Institute for Nanoscale Science
and Technology, Rice University, Houston, Texas 77005, USA **

First-principles calculations for carbyne under strain predict that the Peierls transition from symmetric cumulene to broken-symmetry polyyne structure is enhanced as the material is stretched. Interpretation within a simple and instructive analytical model suggests that this behavior is valid for arbitrary 1D metals. Further, numerical calculations of the anharmonic quantum vibrational structure of carbyne show that zero-point atomic vibrations alone eliminate the Peierls distortion in a mechanically free chain, preserving the cumulene symmetry. The emergence and increase of Peierls dimerization under tension then implies a qualitative transition between the two forms, which our computations place around 3% strain, whereupon the conductivity of carbyne sharply decreases. Thus, zero-point vibrations and mechanical strain jointly produce a change in symmetry resulting in the transition from metallic to insulating state. In any practical realization, it is important that the effect is also chemically modulated by the appropriate choice of terminating groups. Our findings are promising for applications such as electromechanical switching and band gap tuning via strain, and besides carbyne itself, they directly extend to numerous other systems that show Peierls distortion.

Carbyne—the linear allotrope of carbon—is perhaps one of the most unusual materials due to its ultimate one-atom thinness. Although this elusive material is notoriously hard to prepare and has been perceived as exotic or even completely fictitious, the development of methods to synthesize it proceeds at a steady rate, with input from both experimentalists and theoreticians [1–7]. Among the most notable recent achievements, chains with length of up to 44 atoms [8] and such complex molecular mechanisms as carbyne-based rotaxanes [9, 10] have been synthesized. This progress is driven by carbyne’s attractive physical properties such as unusual electrical [11, 12] and mechanical behavior [13], or its large specific area [14]. Accordingly, a better theoretical understanding of this material is becoming more and more relevant.

It has long ago been established by the quantum chemistry community [15] that carbyne undergoes the Peierls transition [16–19] that converts it from the cumulene ($=C=C=$)_n to the polyyne ($-C\equiv C-$)_n form. More recently, it has been suggested that the zero-point (ZP) vibrations may be able to overcome the Peierls instability and restore the nonalternating bond pattern in carbyne [20], as well as in another canonical example of Peierls instability, polyacetylene [21]. Since the symmetric and broken-symmetry forms have very distinct electronic properties (metallic and semiconducting, respectively), investigations of this effect are important from not just the fundamental chemical physics perspective, but also practically relevant for the field of conducting polymers.

Recently, we have found through first-principles calculations that stretching carbyne produces a number of interesting consequences [13] (also observed experimentally after the present study had been completed [22]). The bond length alternation (BLA), defined as the difference between the single and triple bond length, the energy of Peierls distortion, and the band gap all increase with strain. The latter is counterintuitive because normally one would expect strain to result in a weaker orbital overlap, and hence, smaller $\pi - \pi^*$ band splitting. The BLA increase could counter this effect via symmetry breaking–induced increase of this splitting. However, the BLA increase itself can not be easily explained within a classical ‘balls-and-springs’ mechanical representation of carbyne.

Thus, we begin with an exploration of the effect of strain on the Peierls transition. We use a simple analytical model to explain why strain amplifies the Peierls effect. Then, we investigate through first-principles Born–Oppenheimer potential energy surface calculations how the atomic vibrations manifest themselves in equilibrium and under strain, confirming the earlier predictions that the Peierls effect at zero strain is too weak, so that the transition barrier lies well below the ZP vibrational level. Since this barrier is increased by strain, we arrive at the prediction of a strain threshold whereupon carbyne transitions from the ZP vibrations– to Peierls instability–dominated regime, accompanied by a sharp change in electrical conductivity. Our first-principles numerical analysis validates this prediction, placing this transition around $\sim 3\%$ strain (1.5–5.5%). Besides carbyne, our findings naturally suggest that this novel physical effect must also be observable in other one-dimensional systems showing Peierls-transition behavior, such as conducting

*Electronic address: biy@rice.edu

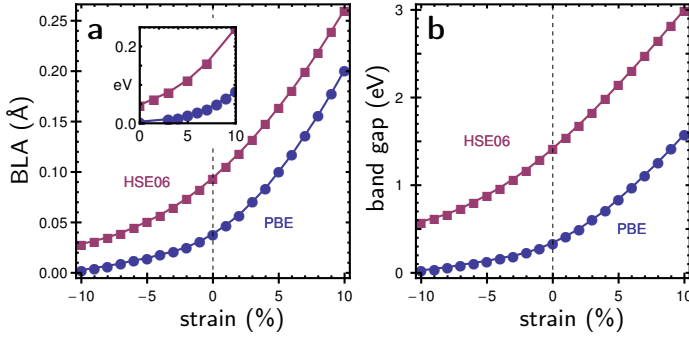


FIG. 1: The (a) bond length alternation and (b) band gap of carbyne as a function of strain using the **PBE** and **HSE06** density functionals. The inset in (a) shows the polyynic-cumulenic energy difference as a function of strain (Peierls barrier).

polymers or carbon nanotubes [23].

We begin by presenting our first-principles data showing the amplification of the Peierls instability under tension. Fig. 1 (a) plots the BLA as a function of strain, and the corresponding energy difference between alternating (polyynic) and nonalternating (cumulenic) structures is plotted in the inset. The band gap dependence on strain is shown in Fig. 1 (b). The Peierls distortion is known to be extremely sensitive to the electronic exchange interaction and, in particular, poorly described by regular density functional theory [24], therefore the calculations were repeated using two methods: (blue) the PBE generalized-gradient density functional [25, 26] and (purple) the HSE06 hybrid functional that includes exact exchange [27, 28]. All Fig. 1 plots conspicuously demonstrate the same universal behavior of increase with strain (also observed in high-level GW calculations [13, 22]).

Clearly, the effect observed so pronouncedly in Fig. 1 data calls for an explanation. We can understand the behavior of Peierls transition under strain with the aid of the following simple Kronig-Penney type model. Consider a chain with two atoms per period a with coordinates $x_1 = 0$ and $x_2 = (a - b)/2$, where b is the BLA. The atoms are represented as attractive Dirac delta functions, and the potential in the unit cell is $V(x) = -\delta(x - x_1) - \delta(x - x_2)$. The textbook expression for the electronic part of the Peierls effect is [29] $E_e \propto V_k^2 \log |V_k| / \hbar k$, where k is the Brillouin zone edge ($k = \pi/a$) and V_k is the corresponding Fourier component of the lattice potential. For our delta-function model, it is simply $V_k = \sin(\pi b/a)$.

The above electronic contribution is counteracted by the lattice deformation energy, $E_l = Cb^2 + O(b^4)$. The spring constant C generally depends on a in some unknown way. Clearly, C should decrease with strain. For mathematical simplicity, we choose $C \equiv C_0/a$. Now all that remains is to minimize the total energy with respect to the BLA b , the condition for which is $\partial(E_e + E_l)/\partial b = 0$. But, upon examination, one finds that with our choice of model, the derivatives of both

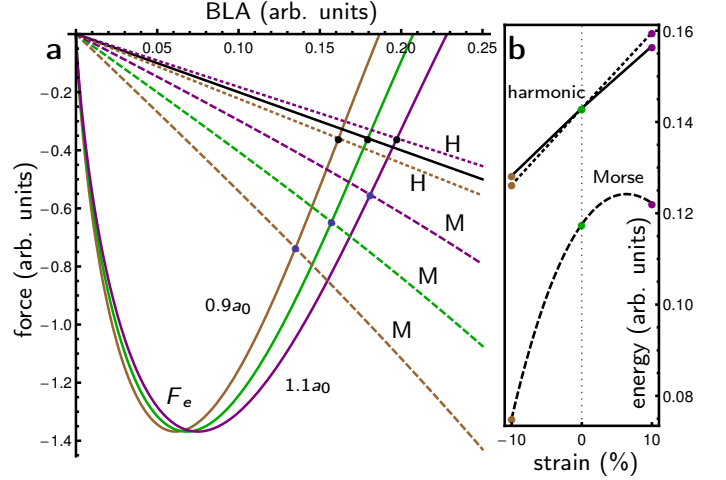


FIG. 2: Analytical model for Peierls instability using $a =$ (yellow) **0.9**, (green) **1.0**, (purple) **1.1** of the equilibrium lattice constant a_0 [arbitrary units] and two models for the lattice deformation potential: strain-dependent-stiffness harmonic spring as in the text (“H”, dotted lines), constant-stiffness harmonic spring (black line), and the Morse potential (dashed lines, “M”). Panel (a) shows the graphical solution for the balance of Peierls (F_e) and restoring forces, and the corresponding Peierls instability energies are shown in (b).

energy terms are only functions of the b/a ratio. This immediately means that $b/a = \text{const}$, and hence, $b \propto a$; that is, the BLA increases with strain.

To demonstrate the robustness of our conclusion with respect to changes in the $C(a)$ dependence, Fig. 2 (a) illustrates the graphical solution for the balance of the electronic driving force of Peierls instability (solid curves colored according to the strain) and the restoring forces, using the harmonic $C \equiv C_0/a$ model (dotted lines, “H”), a constant spring stiffness C_0/a_0 (solid black line), and the Morse potential (dashed lines, “M”). Evidently, the effect of BLA increase with strain should hold for essentially any reasonable form of the restoring force potential. Finally, Fig. 2 (b) plots the corresponding energy differences between polyynic and cumulenic forms, demonstrating that our model can indeed explain all three plots of Fig. 1. (We note that the Morse potential, due to its rapid softening with length, can produce a nonmonotonic dependence of distortion energy at large tensile strain—see dashed line in Fig. 2 (b).)

Up until now, we have confined ourselves to the static picture of carbon atoms. Within this picture, only the cumulenic form of carbyne is stable (at low temperatures), and stretching it produces merely *quantitative* changes in the band gap—a phenomenon known previously in solid state physics. However, as we demonstrate below, the inclusion of quantized nuclear motion changes the picture dramatically. If ZP vibrations can overpower the Peierls instability in mechanical equilibrium and restore the symmetric metallic structure as previously suggested [20, 21], then, considering this together with our above

findings, one is led to expect that at some critical strain value, the stronger Peierls instability may reverse this phenomenon—causing a *qualitative* change in properties. Our calculations indeed confirm this.

For the vibrational analysis, the Born–Oppenheimer potential energy surface scans along the BLA coordinate were computed with the PBE and HSE06 functionals, yielding the potential energy surface (PES) profiles $E_a(b)$ as the lattice constant a was increased from its equilibrium value. Because of the strong anharmonicity of the “inverse McDonald’sTM” ω -shaped PES profiles, we had to turn to numerical calculations of the vibrational levels at each strain value. We utilized the Fourier grid Hamiltonian method [30, 31] which had been previously successfully used to study polyacetylene in a similar context [21]. Following the previous studies, we assume that the longitudinal vibrations can be decoupled from the two transverse phonons and treated separately, which is justified by the non-negligible bending stiffness of carbyne [13, 32–34]. (Indeed, the inclusion of transverse vibrations and dispersion does not change our conclusions, as detailed in the Supplementary Materials.) We used a uniform grid of 250 points in $-0.4 \text{ \AA} < b < 0.4 \text{ \AA}$, using interpolation of DFT-computed values of energy, and 6.005 a.m.u.—the reduced mass of two carbon atoms—for the oscillator mass.

The results are presented in Fig. 3, which is the central figure of this paper. The red lines show the ω -shaped PES (in eV), blue lines denote the computed vibrational levels with filling below the zeroth level, and the green lines plot the ZP wavefunction, as computed using the HSE06 functional. The right panels show the reconstructed real-space densities of nuclei at the respective strain values. The profile along the horizontal axis is taken directly from the vibrational wavefunctions, and an arbitrarily chosen value of 0.12 \AA is used for the transverse broadening.

Clearly, the mechanically relaxed system has a single wavefunction maximum, corresponding to the cumulene structure of carbyne—although the PES has a local maximum in this point. In accordance with the above discussion, the maximum (‘Peierls barrier’) rises with strain, and at 3%, the wavefunction already has a slight dip in the center, resulting in a picture of ‘elongated’ atoms. At 7% strain, the ground-state wavefunction is clearly separated in two blobs, and the first excited level (antisymmetric with a node in the middle) approaches the ground-state level, indicative of the transition to the double-well potential-like regime. Finally, at 10% strain, the first excited level is well below room-temperature $k_B T$ relative to the ground state, as in two independent potential wells. The second level dives below the Peierls barrier, and the third begins to approach it. (At 15% strain these two also become degenerate; data not shown.)

The above-described sequence of events has a very profound consequence. As the strain is increased, carbyne transitions from the conducting electronic behavior of cumulene to the nonconductive polyne structure with its

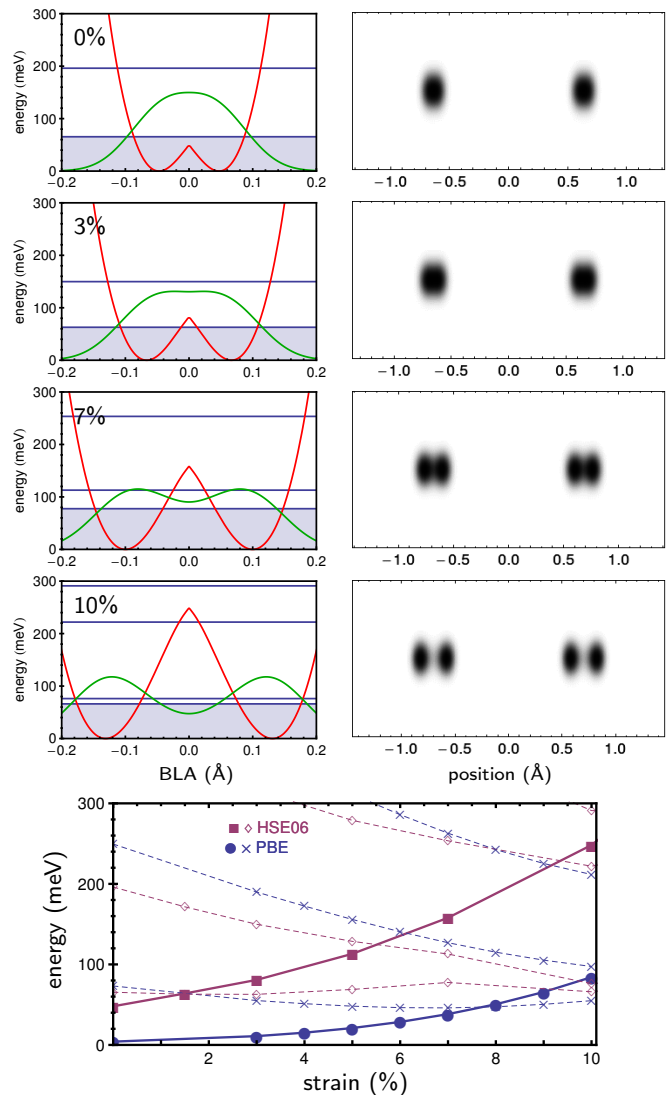


FIG. 3: (left) Evolution of the vibrational level structure of carbyne with strain: from 0% to 10%. Red lines represent the ω -shaped **potential energy** as a function of BLA, calculated with the HSE06 density functional. Blue lines show the **vibrational levels** (the filled region is below the ZP level). Green lines show the **ZP wavefunction**. (right) Real-space atomic density distributions calculated based on the ZP wavefunction. The plot in the bottom shows the strain dependence of Peierls barrier (circles, **PBE**; squares, **HSE06**) and vibrational levels (colored × and diamond symbols).

sizable band gap (see Fig. 1 (b)). The exact point at which this happens is not clear from Fig. 3 plots, and direct phonon-coupled electronic transport calculations are infeasible. However, an approximate criterion can be suggested basing on the bottom plot in Fig. 3, which shows the joint evolution of the Peierls barrier and vibrational levels under strain. The wavefunction starts to acquire the dual-maximum character when the ground-state level dives below the Peierls barrier, and we can consider the transition to be well over by the time the same happens to the first excited level. As seen in the bottom of Fig. 3,

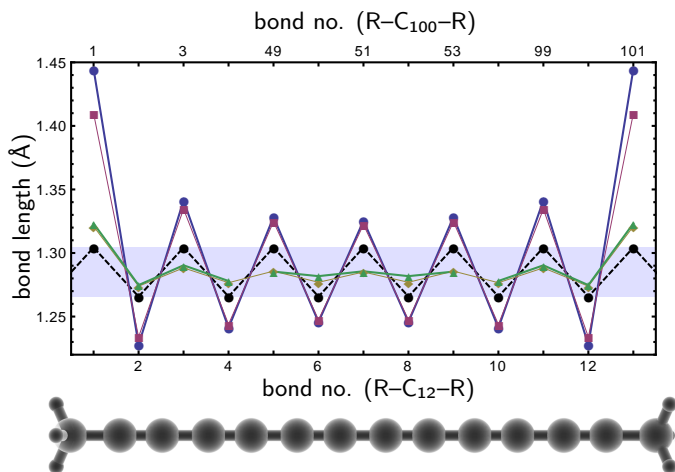
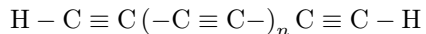


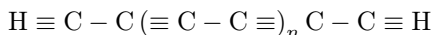
FIG. 4: Effect of endgroups on the BLA in carbyne. Termination of the chain with sp^3 groups (methyl $-\text{CH}_3$ and phenyl $-\text{C}_6\text{H}_5$) increases the BLA, whereas the sp^2 methylene group ($-\text{CH}_2$) decreases it, as compared to an unterminated infinite chain (black dashed line). The data for **12-** and **100-atom** chains show weak decrease of BLA with chain length away from the ends with methylene termination.

these two events happen at the 1.5% and 5.5% strain values, respectively, which is a reasonably mild strain from the mechanical point of view. (PBE gives 8% and slightly above 10%, correspondingly.)

So far our calculations treated carbyne as an infinite chain. In a real experiment, however, the ends of finite carbyne chains inevitably represent special points that might affect the picture laid out above. (Note that our predictions should still apply directly to carbyne rings.) The PES of infinite carbyne contains pairs of minima and is invariant under translation by half a unit cell (assuming polyynes form), which corresponds to the exchange of triple and single bonds. But, as a simple example, the two *finite* structures described by chemical formulae



and



are, clearly, very nondegenerate, because hydrogen cannot form stable triple bonds with carbon. On the other hand, the use of end-groups that locally favor the cumulene structure, such as methylene $=\text{CH}_2$, could be expected to be less disruptive. The effect of end-groups will clearly have a different strength for different moieties, and a comprehensive investigation of the variety of possibilities is an extensive task (further aggravated by complexity of collective atomic motions in such many-atom systems) that is beyond the scope of the present study. However, simply looking at how the BLA depends on the endgroup type in finite carbyne fragments already provides a useful glance into the issue.

The results of our finite-chain calculations with different terminating groups are presented in Fig. 4. The strip from 1.27 to 1.30 Å denotes the bond lengths in the ideal infinite polyynes chain (ignoring the ZPV). The bond lengths in the sp^3 -terminated systems ($-\text{CH}_3$, $-\text{C}_6\text{H}_5$) fall outside this strip, showing the enhanced polyynes-like character of the system. On the other hand, sp^2 -type termination with $-\text{CH}_2$ reduces the BLA effectively to zero (< 0.01 Å for a 12-atom chain and < 0.005 Å in the middle of a 100-atom chain), suggesting that this type of passivation does not significantly disrupt the potential energy picture shown in Fig. 3. Thus, the use of end-groups that locally favor the cumulene structure should allow our predictions to be observed. (Indeed, such groups are preferable from the electronics applications standpoint in order to provide metallic ‘leads’ at the ends of the chain.) In summary, we see that in experimental realizations, the effect may be destroyed by improper chemical termination of carbyne chains, and thus, precise control over both the tension and chemistry is essential.

Our findings regarding the importance of vibrations in carbyne add another example of a system where quantum effects in the motion of atoms have big consequences. This notably contrasts with the physicist’s intuition saying that the carbon atom is too heavy for quantum effects to be significant, yet its mass is compensated for by the extreme mechanical stiffness of the carbyne lattice [13]. Carbyne represents one more case where vibrations, even at zero temperature, may stabilize a material in a configuration that is not even a local minimum of the Born–Oppenheimer PES [35]. Recently, quantum-mechanical effects in the nuclear motion were demonstrated to play roles in the dynamics of such systems as vacancies in graphene [36] or dislocations in 3D crystals [37]. However, to our knowledge, carbyne (and likely, by analogy, polyacetylene) is the first example where such effects can lead to *qualitative* differences in the material’s behavior—here, electronic conductivity.

In conclusion, we have explored how the Peierls instability of linear carbon chains is enhanced by strain using first-principles calculations, and explained it with a simple analytical model. At zero strain, the Peierls instability in carbyne is too weak to overcome the quantum zero-point vibrations, and the stable structure corresponds to the metallic cumulene rather than insulating polyynes—despite the lower potential energy of the latter structure. However, the enhancement of Peierls instability results in the reversal of this effect, and carbyne starts to demonstrate the polyynes-like character of the nuclear wavefunction, switching from the conducting to insulating behavior around $\sim 3\%$ strain. This novel effect naturally applies to carbyne rings and other one-dimensional systems such as polyacetylene or carbon nanotubes. Our findings are important both as an interesting fundamental physical effect and highly practically relevant for the science of conducting polymers. Although at present carbyne remains a highly exotic material, its unique proper-

ties will continue to fuel the community effort to achieve its synthesis in practically useful quantities.

The computations were performed using the VASP

code [38] with projector-augmented wave basis sets [39, 40], using the Data Analysis and Visualization Cyberinfrastructure funded by NSF under Grant OCI-0959097.

-
- [1] *Polyynes : synthesis, properties, and applications*, edited by F. Cataldo (CRC Press, Boca Raton, 2005).
 - [2] C. Jin *et al.*, *Phys. Rev. Lett.* **102**, 205501 (2009).
 - [3] E. Hobi, R. B. Pontes, A. Fazzio, and A. J. R. da Silva, *Phys. Rev. B* **81**, 201406 (2010).
 - [4] E. Erdogan *et al.*, *Phys. Rev. B* **83**, 041401 (2011).
 - [5] G. Casillas *et al.*, *submitted*.
 - [6] B. Yakobson, M. Campbell, C. Brabec, and J. Bernholc, *Comput. Mater. Sci.* **8**, 341 (1997).
 - [7] H. E. Troiani *et al.*, *Nano Lett.* **3**, 751 (2003).
 - [8] W. Chalifoux and R. Tykwinski, *Nature Chem.* **2**, 967 (2010).
 - [9] L. D. Movsisyan *et al.*, *Org. Lett.* **14**, 3424 (2012).
 - [10] N. Weisbach *et al.*, *Chem. Commun.* **48**, 7562 (2012).
 - [11] K. H. Khoo *et al.*, *Nano Lett.* **8**, 2900 (2008).
 - [12] Z. Zanolli, G. Onida, and J.-C. Charlier, *ACS Nano* **4**, 5174 (2010).
 - [13] M. Liu *et al.*, *in preparation*.
 - [14] P. B. Sorokin *et al.*, *Nano Lett.* **11**, 2660 (2011).
 - [15] M. Kertesz, J. Koller, and A. Azman, *J. Chem. Phys.* **68**, 2779 (1978).
 - [16] R. E. Peierls, *Annalen der Physik (Leipzig)* **4**, 121 (1930).
 - [17] R. E. Peierls, *Quantum Theory of Solids* (Clarendon Press, Oxford, 2001).
 - [18] H. Frohlich, *Proc. R. Soc. London. Ser. A.* **223**, 296 (1954).
 - [19] T. Kennedy and E. H. Lieb, *Phys. Rev. Lett.* **59**, 1309 (1987).
 - [20] S. Tongay *et al.*, *J. Phys. Condens. Matter* **17**, 3823 (2005).
 - [21] B. S. Hudson and D. G. Allis, *J. Mol. Struct.* **1032**, 78 (2013).
 - [22] O. Cretu *et al.*, arXiv:1302.5207 (2013).
 - [23] J. W. Mintmire, B. I. Dunlap, and C. T. White, *Phys. Rev. Lett.* **68**, 631 (1992).
 - [24] D. Jacquemin *et al.*, *J. Phys. Chem. A* **110**, 5952 (2006).
 - [25] J. P. Perdew, K. Burke, and M. Ernzerhof, *Phys. Rev. Lett.* **77**, 3865 (1996).
 - [26] J. P. Perdew, K. Burke, and M. Ernzerhof, *Phys. Rev. Lett.* **78**, 1396 (1997).
 - [27] J. Heyd, G. E. Scuseria, and M. Ernzerhof, *J. Chem. Phys.* **118**, 8207 (2003).
 - [28] J. Heyd, G. E. Scuseria, and M. Ernzerhof, *J. Chem. Phys.* **124**, 219906 (2006).
 - [29] L. Mihály and M. C. Martin, *Solid State Physics: Problems and Solutions* (John Wiley & Sons, New York, 2009).
 - [30] C. C. Marston and G. G. Balint-Kurti, *J. Chem. Phys.* **91**, 3571 (1989).
 - [31] R. D. Johnson III, Fourier Grid Hamiltonian 1D Program, http://www.nist.gov/mml/csd/informatics_research/fourier_grid_hamiltonian.cfm
 - [32] L. Ravagnan *et al.*, *Phys. Rev. Lett.* **102**, 245502 (2009).
 - [33] Y. H. Hu, *J. Phys. Chem. C* **115**, 1843 (2011).
 - [34] I. E. Castelli, P. Salvestrini, and N. Manini, *Phys. Rev. B* **85**, 214110 (2012).
 - [35] P. Souvatzis, O. Eriksson, M. I. Katsnelson, and S. P. Rudin, *Phys. Rev. Lett.* **100**, 095901 (2008).
 - [36] Z. S. Popović, B. R. K. Nanda, and S. Satpathy, *Phys. Rev. B* **86**, 085458 (2012).
 - [37] L. Proville, D. Rodney, and M.-C. Marinica, *Nature Mater.* **11**, 845 (2012).
 - [38] G. Kresse and J. Furthmüller, *Phys. Rev. B* **54**, 11169 (1996).
 - [39] P. E. Blöchl, *Phys. Rev. B* **50**, 17953 (1994).
 - [40] G. Kresse and D. Joubert, *Phys. Rev. B* **59**, 1758 (1999).